Macromolecules
ARTICLE

Macromolecules **2009**, *42*, 9581–9591 **9581**
DOI: 10.1021/ma901890f

Local Dynamics and Hydrogen Bonding in Hyperbranched Aliphatic Polyesters

I. Tanis and K. Karatasos*

Laboratory of Physical Chemistry, Department of Chemical Engineering, Aristotle University of Thessaloniki, 54124 Thessaloniki, Greece

Received August 26, 2009; Revised Manuscript Received October 22, 2009

ABSTRACT: We report results from fully atomistic molecular dynamics simulations of commercially available aliphatic hydroxyl-terminated hyperbranched polyesters of two different architectures/sizes in the bulk, exploring dynamic mechanisms associated with their physical behavior as it has been described by pertinent experimental techniques. Particular emphasis is given on the role of the hydrogen-bonding capabilities of the examined systems and the impact on their local dynamic response. Analysis of the simulation results reveals that certain key aspects of their unique behavior, such as the molecular weight dependence of local group reorientation as well as the more restricted motion of these moieties in low-generation polyesters, can be explained by considering the distinct hydrogen-bonding pattern, which is realized at the intra- and intermolecular levels. This interconnection is shown to be realized through a coupling mechanism of local bond relaxation with the time scale pertinent to the formed hydrogen bond network. Quantitative accounts are provided for the relative percentage of the different kinds of hydrogen bonds as well as for their corresponding lifetimes. The detail afforded by the present work provides new insight into the structure/properties relation of such molecules and offers new ground for the interpretation of relevant experimental findings.

1. Introduction

Understanding the structure/properties relation in polymeric systems is a milestone toward designing materials with tailor-made functionality. This task becomes more demanding when polymer molecules bear complex architectures with additional functionalities, as in the case of hyperbranched polymeric materials.[1,2] Apart from characteristics such as the size and the total molecular weight, which should be taken into account in common linear polymers, attributes like the branching pattern, the number and the relative location of the functional groups within the branched structure, greatly affect their properties.[3−7] Probably the most decisive part regarding the physical behavior of hyperbranched systems is associated with the nature of their surface functional groups, as has been demonstrated in several experimental[8−13] and computational studies.[14−17] Substitution of their peripheral groups may alter their mechanical,[8,11,18−21] thermal,[20,22] and thermodynamic behavior.[23−27]

Hyperbranched polyesters belong to a category of highly branched polymers, the synthesis of which has been nowadays well formulated to the point at which they can be produced on a relatively large scale,[28] whereas alteration of their surface groups can be commonly performed by following now standard procedures.[1,29,30] One of the most widely used families of such polymers is the hydroxyl-terminated aliphatic polyesters, which, because of their commercialization, their competitive cost, and their advantageous properties, have become the object of intense scientific and industrial interest.[31−34] The hyperbranched polyesters bearing the commercial name Boltorn[28] are now considered to be key ingredients in many nanoscale applications, including biomedical uses.[21,32,33,35]

Because of their potential for such applications, several experimental investigations have been performed exploring their structure/properties relation.[8,11,18,20,29,36−42] In several instances during these studies, investigators observed a rather uncommon physical behavior, such as the molecular weight dependence of the time scales describing very local dynamic processes (e.g., the β-process or the γ relaxation associated in these polymers with the surface−OH group motion[36,42]) that assume unusually high activation energies[36,41,42] or different activation energies for presumably identical motional mechanisms depending on the size and the topology of the examined molecule.[41,42] These phenomena as well as other discrepancies observed between experiments performed in similar samples from different experimental groups,[11,37] were attributed mainly to the existence of a significant degree of inter- and intramolecular hydrogen bonding, which may decisively affect the dynamic response of the systems.[8,18]

The aim of the present work is to provide a closer view of the dynamic behavior on a local scale in relation to the size/topology of the examined models and to their hydrogen-bonding capabilities. To this end, we have performed fully atomistic molecular dynamics (MD) simulations in the bulk for hydroxyl-terminated polyesters of two different (pseudo)generations over a wide temperature range above the glass-transition temperature. Because of the atomistic resolution afforded by the adopted simulation method, we were able to identify in a quantitative manner the extent of the formation of different kinds of hydrogen-bonded pairs of either intra- or intermolecular nature together with their relative lifetimes as well as their impact on local motion in conjunction with the size/topology of the examined polymers. To our best knowledge, this is the first study of this nature in these polymers and over such a wide temperature range.

2. Simulation Details

2.1. Examined Systems. Systems of two different (pseudo)generations, namely, of generation 2 and 3, were examined, corresponding to the theoretical structures of the commercial aliphatic OH-terminated polyester family

*Corresponding author. Tel: +30-2310-995850. Fax: +30-2310-996222. E-mail: karatas@eng.auth.gr.

© 2009 American Chemical Society

Published on Web 11/02/2009

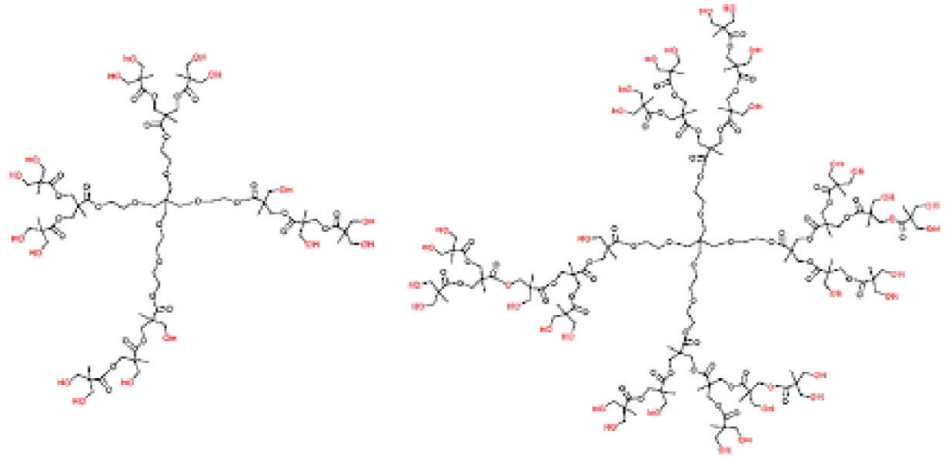

Figure 1. Molecular architectures of the 2nd (left) and the 3rd (right) generation aliphatic polyesters studied in the present work, corresponding to the H20 and H30 Boltorn theoretical structures.[28]

Table 1. Characteristics of the Simulated Models

code	M_w (g/mol)	−OH groups	molecules per model	T_g (°C)
H20	1750	16	35	30
H30	3608	32	20	35

referred to as H20 and H30, respectively (Boltorn, Perstorp company[28]), as illustrated in Figure 1.

Table 1 lists the characteristics of the simulated models. The glass-transition temperatures are provided by the company but also measured experimentally by means of dynamic mechanical analysis (DMA) in systems bearing theoretical structures identical to the ones studied here.[41]

2.2. Simulation Protocol. We generated fully atomistic melt samples of Boltorn H20 and H30 containing 35 and 20 molecules, respectively, through the use of the amorphous cell algorithm.[43] Energetic parameters were taken from the AMBER[44] forcefield, containing terms for bonded (bond stretching, angle bending, torsional rotation) and nonbonded interactions (van der Waals, electrostatic), according to eq 1

$$E_{\text{total}} = \sum_{\text{bonds}} K_R(R-R_0)^2 + \sum_{\text{angles}} K_\theta(\theta-\theta_0)^2 + \sum_{\text{dih.}} \frac{V_n}{2}[1+\cos(n\phi-\delta)] + \sum_{i<j}\left[\frac{A_{ij}}{R_{ij}^{12}} - \frac{B_{ij}}{R_{ij}^{6}}\right] + \sum_{\text{H-bonds}}\left[\frac{C_{ij}}{R_{ij}^{12}} - \frac{D_{ij}}{R_{ij}^{10}}\right] + E_{\text{elec.}} \quad (1)$$

The adopted force field has been proven to describe rather satisfactorily certain aspects of the physical behavior of other hyperbranched polymers in past computational studies.[45−47] On the basis of its successful combination with the adopted forcefield,[48−50] the assignment of partial charges was performed through the Gasteiger method,[51] whereas Coulombic interactions were evaluated by full Ewald summation. Dispersive interactions were described by a 12−6 Lennard-Jones potential (with a cutoff radius of 10 Å), whereas hydrogen bonding interactions between proton acceptors and hydrogens of hydrogen bond donors were modeled by a 12−10 potential term.[44,52,53]

In the first stage of the simulation, initial configurations of the melt samples of both polyesters were constructed at an elevated temperature. The models were then subjected to successive MD[54] cooling steps of 50 K in the isobaric−isothermal ensemble. The systems spent 200 ps (in 1 fs steps) at each cooling step, followed by 100 000 to 150 000 steepest-descent and conjugate-gradient energy minimization cycles. Before proceeding to production runs in the microcanonical ensemble (NVE), 2 ns of further MD runs in the isobaric−isothermal (NPT) ensemble were performed at each temperature, after which the potential energy, the specific volume, and the radius of gyration of the polymers were stabilized. At the final part of the simulation, we conducted production runs of 5 to 15 ns (depending on temperature) in the NVE ensemble with a time step of 1 fs and frame-saving frequency of 1 ps. Because bond orientational dynamics and average lifetimes of hydrogen bonds could be realized even on a subpicosecond time scale, additional runs were performed with a frame-saving frequency of 2 fs.

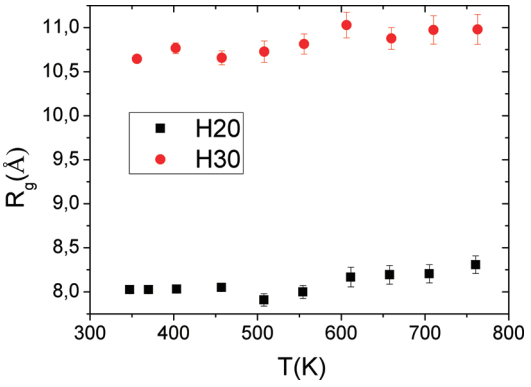

Figure 2. Variation of the average radius of gyration of the simulated systems as a function of temperature. Error bars correspond to the standard deviation.

Figure 2 depicts the dependence of the radius of gyration of the examined systems on temperature, where a very weak variation can be noticed. (At all temperatures and for both systems, the radius of gyration remains at least 5 times smaller compared with the dimension of the simulation box.)

Figure 3 shows snapshots of equilibrated melts for the two examined systems.

To verify the appropriateness of the forcefield and the simulational protocol adopted for the representation of the examined systems, we have compared results from our simulations with available PVT experimental data.[55]

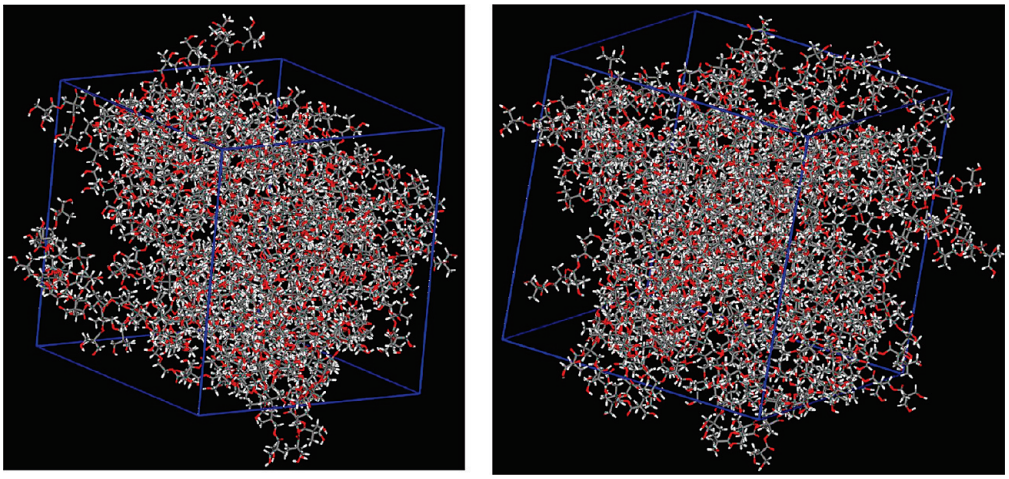

Figure 3. Snapshots of equilibrated melts for the H20 (left) and H30 (right) models at $T = 457$ K.

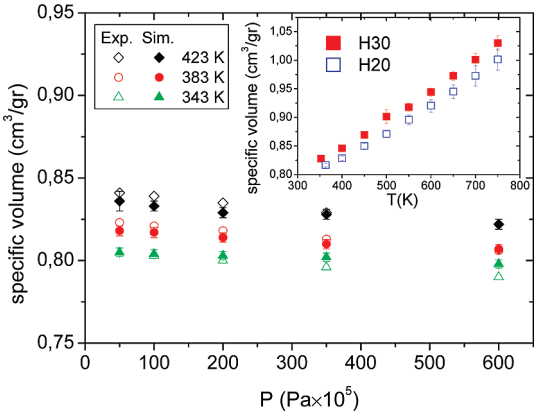

Figure 4. Comparison of simulation PVT points of the H20 polyester with available experimental data.[55] Inset shows the temperature dependence of the specific volume of both examined models under ambient pressure.

Figure 4 shows the comparison between results from constant-pressure constant-temperature simulations and experimental data for the H20 system.[55] Inset displays the temperature dependence of the examined models at $p = 1$ atm from NPT MD runs.

Evidently, simulation results are in good agreement with experimental data. As shown in the inset, no change of slope is observed for both systems over the examined temperature range; that is, no glass-transition temperature is detected, as is also anticipated from the T_g values in Table 1. The specific volume of the low generation model H20 appears to be slightly lower than that of the H30 system at high temperatures, but the two sets of points seem to approach as temperature decreases. This trend is consistent with the experimental observation that the two systems in the bulk and at room temperature assume practically the same density.[8]

3. Results and Discussion

Previous investigations in hyperbranched polyester systems of the same family as those studied here revealed the existence of two sub-T_g dynamic processes denoted as β and γ, apart from the α-relaxation mechanism related to the glass−rubber transition.[20,36,41] The two subglass processes exhibited an Arrhenius behavior and were associated with the ester-group reorientation (β) and the motion of the hydroxyl terminal groups (γ), respectively.[20,36,42] The chemical nature of the surface end groups in these systems was found to play a crucial role not only in their local dynamic behavior[20] but also in their macroscopic rheological response.[8,11]

Particularly for the hydroxyl-terminated systems, it was found that a hydrogen-bond network was formed,[56] the characteristics of which were sensitive to the thermal treatment of the sample.[18,39] The time scale related to the annealing process at the selected temperatures, which was necessary to affect significantly the thermal and mechanical properties of the OH-terminated polyesters, amounted typically to several thousands of seconds.[18,39] The time scales relevant to the cooling procedure followed in the simulations (see the previous section) as well as the time window at which the produced trajectories extended were several orders of magnitudes shorter than those reported in the annealing experiments. Therefore, the simulation "measurements" should be considered to be performed in quenching temperature steps with the systems remaining at each temperature for only a short period of time so that the effects associated with the slow formation of the hydrogen bonds would not be present. The self-consistency of the simulation results, as will be presented in the forthcoming sections, attests to the appropriateness of such a procedure for a fair representation of the systems at different temperatures.

3.1. Local Dynamics. To probe dynamics on a local length scale, we have calculated the second-order time correlation functions describing the reorientation of characteristic bonds, $C(t)$

$$C(t) = \frac{1}{2}\langle 3[\hat{\mathrm{h}}(t)\cdot\hat{\mathrm{h}}(0)]^2 - 1\rangle \qquad (2)$$

The unit vectors lie along the direction of the examined bond. To check possible effects related to the hydrogen-bond formation in local bond relaxation, we have monitored three different kinds of bonds: (a) C−C bonds where neither carbon atom belongs to a carbonyl group, (b) C−O bonds between carbon atoms and hydroxyl oxygens (OH), and (c) hydroxyl hydrogen (HO)−hydroxyl oxygen (OH) bonds. Because hydroxyl oxygens and carbonyl oxygens actively participate in the hydrogen-bond network,[56] orientational dynamics of such bonds could be affected by the extent of hydrogen bonding and the longevity of the relevant hydrogen bonds.

We performed analysis of the resulting dynamic spectra by determining the distribution of exponential relaxation times (DRTs).[57,58] According to this procedure, a dynamic correlation function is considered to be a continuous

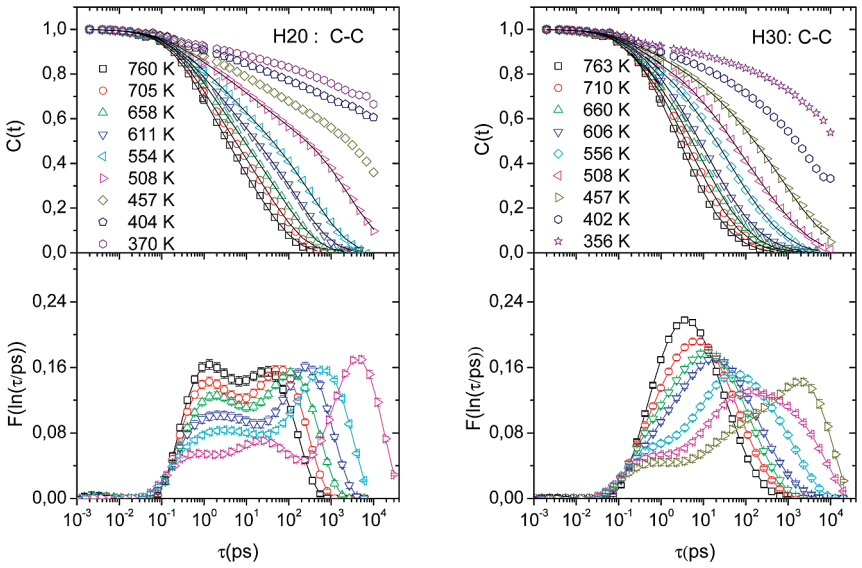

Figure 5. Bond orientational correlation functions (upper panels) together with the corresponding DRTs (lower panels) of the H20 (left) and the H30 (right) models. The lines through the points in upper panels correspond to the fits according to eq 2. DRTs are shown only for spectra for which almost complete decorrelation has been accomplished within the examined time window.

superposition of single exponential processes

$$C(t) = \int_{-\infty}^{\infty} F(\ln(\tau))\mathrm{e}^{-t/\tau}\, \mathrm{d}\ln\tau \qquad (3)$$

where F represents the obtained DRT. Different dynamic processes, well-separated in the time domain, appear as different peaks in the distribution. Corresponding relaxation times are estimated via the first moment of the calculated distribution function, $F(\ln(\tau))$, over the time window of the relevant peak. If the entire distribution is taken into account, then an overall average relaxation time equivalent to integrating the dynamic function can be calculated instead. For a nearly symmetric peak, the location of the maximum provides a good estimation of the corresponding relaxation time. The area under each peak denotes the relative contribution of each process to the decorrelation of the dynamic function.

Between the aforementioned kinds of bonds, the C−C bond can be characterized as a "backbone" bond because the atoms that constitute it do not belong in any group at the extremity of the hyberbranched structure. In addition, the considered carbon atoms are not expected to influence the hydrogen bonding behavior. On the contrary, the C−OH bond represents a bond at the extremities of the molecule, whereas the HO−OH bond is the outermost bond of the structure. Because both of the latter bonds consist of hydroxyl oxygen, it is anticipated that hydrogen bonding might affect their dynamics. This notion should be kept in mind for the interpretation of the respective dynamic spectra.

3.1.1. Backbone Bond Relaxation. Figure 5 displays the bond reorientational correlation functions of the C−C bond, together with the corresponding DRTs.

A visual comparison between the correlation spectra of the two systems reveals that the C−C bond of the H20 model appears to relax at longer times compared with the H30 analogue (compare, e.g., the degree of decorrelation of spectra of the two systems corresponding to close temperatures). This is a rather unexpected result because for other dendritic molecules, it has been found that local relaxations associated with the glass−rubber transition become slower upon an increase in generation number[59−61] (recall that C−C is a "backbone" bond). By focusing on the spectral features of the corresponding DRTs, even more qualitative differences can be noted between the two models. In the H30 systems, the distribution is characterized by a single broad peak at higher temperatures that shifts toward longer times as the temperature decreases, whereas at the lowest temperature analyzed, indications of a much faster and an intermediate peak can be noted. The latter is implied by the appearance of a "shoulder" in the left flank of the slower peak. In contrast, in the H20 sample, DRT spectra appear to be bimodal, even at the highest temperature examined. The slower peak shifts to longer times upon the decrease in temperature, whereas the location of the maxima of the faster one (i.e., its characteristic time) is rather insensitive to temperature changes. At the lowest temperature analyzed, the intermediate peak can be clearly discerned. To interpret the nature of each dynamic process as represented by the different peaks, we must bear in mind the possible dynamic mechanisms that contribute to local bond relaxation. As has been demonstrated in previous studies (see, e.g., ref 47 and references therein), in principle, the main "channels" through which bond reorientation is realized, are (i) an ultrafast (on the order of picoseconds or faster) librational motion of the bond, (ii) an ultraslow process associated with the overall molecular rotation, and (iii) the reorientation of the bond, as dictated by its local environment. Depending on this local environment as well as on the relative distance from the glass-transition temperature, the time scales of these mechanisms could be either well separated (i.e., differing in temporal scale by a decade or more so that they can be resolved as distinct processes[62]) or may appear to be coupled,[47] whereas their relative contribution to the bond relaxation may vary.

Because of the extremely local character of the ultrafast mechanism (in terms of the time scale and the effective displacement of the atoms involved in this motion), it exhibits an almost temperature-independent characteristic time,[61,63] whereas the two slower mechanisms are, in principle, characterized by a stronger temperature dependence.[47,61] At temperatures much higher that the glass transition, depending on the size of the polymer and its flexibility, the overall molecular rotation and the fast

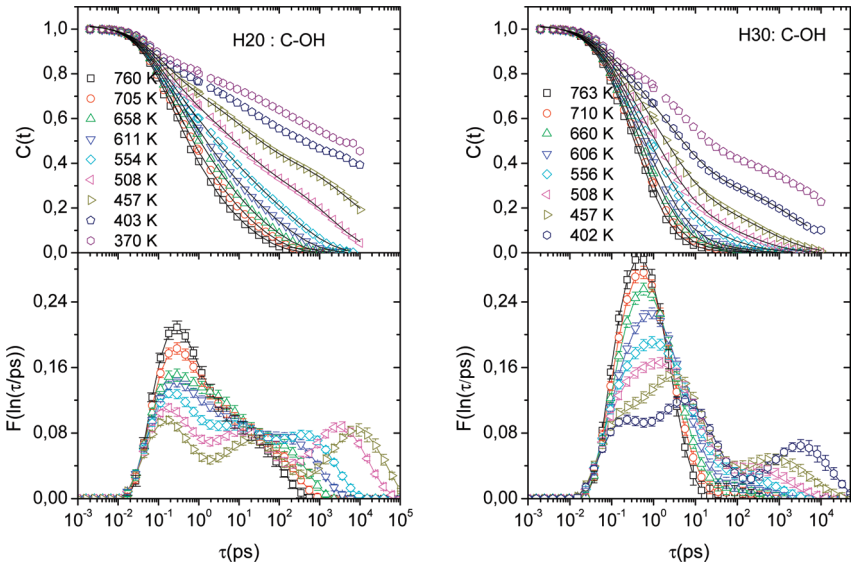

Figure 6. Bond relaxation spectra (upper panels) of the C−OH bond in the H20 (left) and the H30 (right) models. Lines through the points are fits resulting from the DRT analysis. Lower panels present the corresponding DRTs.

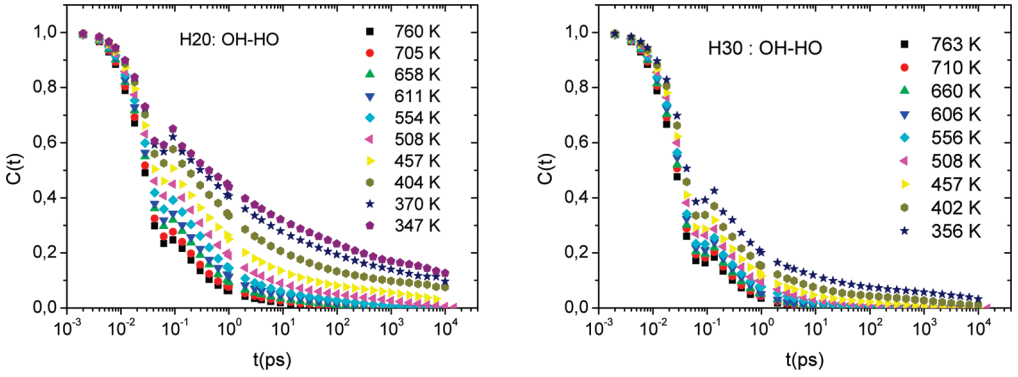

Figure 7. OH−HO bond reorientational spectra for the H20 (left) and the H30 (right) model.

tumbling motion may suffice for an almost complete decorrelation, even of a backbone bond, whereas as the temperature decreases and the overall rotation becomes increasingly slower, the contribution of the intermediate and the ultraslow process becomes more important for the relaxation of a backbone bond.[47]

On the basis of the above picture, it appears that the time scales of the different mechanisms for backbone bond relaxation are separated "earlier", that is, at higher temperatures in the H20 model (so that distinct peaks can be resolved by the DRT analysis at higher temperatures). This finding implies that despite the lower molecular weight and the relatively lower degree of branching assumed by the H20 model[18] (see also Figure 1), local backbone motion in the lower generation polyester experiences a larger degree of constriction compared with that in the larger H30 model at similar distances above the glass transition.

3.1.2. Bond Motion in a Hydrogen-Bond-Capable Surface Group. Figure 6 depicts the temperature dependence of the C−OH spectra for the examined models, together with their DRTs.

As in the case of the C−C bond (Figure 5), the bond spectra describing the H20 system appear to decorrelate with a lower rate than the H30 analogues (compare the degree of decorrelation of the $C(t)$ functions at similar temperatures). In addition, it appears that for both size models, the ultrafast process assumes a higher relative amplitude (compare the areas under the respective peaks); that is, this process contributes to a larger degree to the loss of orientational memory in the C−OH bond as compared with the C−C bond. The latter should be attributed to the higher relative freedom of the C−OH bond that resides to a side group. Exactly because of this attribute of the C−OH bond and because of the particularly local nature of this motion, the molecular-weight dependence of its relaxation time (as follows from the higher degree of decorrelation of the bond spectra in the H20 model) is an intriguing feature.

3.1.3. Bond Motion in the Terminal Hydrogyl Group. Figure 7 shows the bond reorientational spectra for the OH−HO bond at different temperatures for the examined models. Apart from the essentially temperature-independent fast drop of the correlation function, which extends up to ~0.05 ps for both models, a characteristic feature not observed in the previous bond-relaxation spectra (Figures 5 and 6) is an apparent "recorrelation" maximum at ~0.1 ps. Both of these features have recently been observed in OH−HO bond correlation spectra of hydrogen-bonding-capable hyperbranched systems.[47] The reasoning applied in ref 47 can be applied in the case of the HO−OH bonds in polyesters as well. The fast drop can be ascribed to the rapid tumbling motion of the bond, the "recorrelation" maximum can be linked to the time scale on which a fast formation/breaking of the hydrogen bonds takes place, whereas the slower process implied by the "tail" of

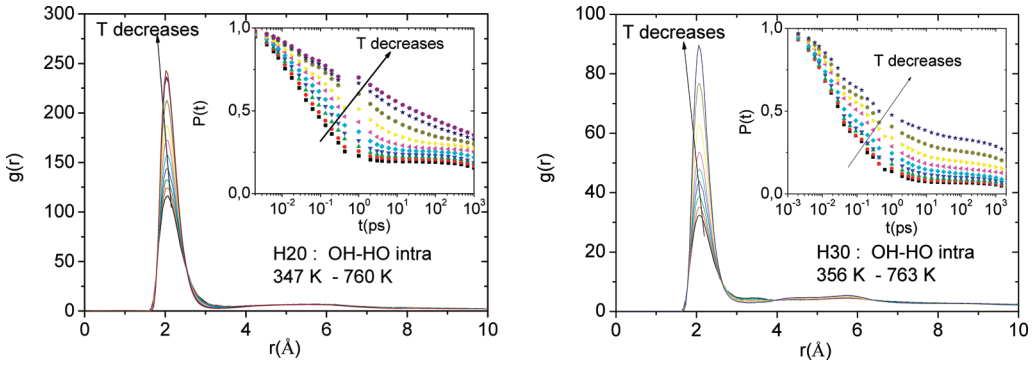

Figure 8. Intramolecular pair distribution functions between hydroxyl hydrogens and hydroxyl oxygens for H20 (left, 347−760 K) and the H30 (right, 356−763 K) models, as a function of temperature. Insets denote the corresponding survival correlations functions (eq 4). Arrows show the direction of the decrease in temperature.

the correlation functions can be associated with the coupling of the OH−HO bond relaxation to local segmental motion.

Comparing the dynamics between the two polyesters, it can be observed that at similar temperatures, the OH−HO bond in the H20 model relaxes on longer time scales. Because for both models the formation of hydrogen bonds is certainly expected and the number of −OH groups in the H20 sample is only marginally higher compared with that in the H30 polyester[41] at a similar density (in the simulated systems the number of hydroxyl groups per unit volume in the H20 exceeds that of the H30 model by about 5% or less depending on the density), the observed difference in the dynamic behavior still remains an open question.

3.2. Hydrogen Bonding. To address the question risen from the behavior of the relaxation of the examined bonds, we have examined the extent and the longevity of the different kinds of hydrogen bonds of intra- and intermolecular nature that could affect local motion in the two polyesters. As has been confirmed by infrared spectroscopy (IR) studies,[18,30,39,56] the most frequent hydrogen-bonded pairs are formed between hydroxyl hydrogens (HO) and hydroxyl oxygens (OH) (the formed hydrogen bond will be symbolized as $OH\cdots OH$ henceforth) and hydroxyl hydrogens (HO) and carbonyl oxygens (O) (this hydrogen bond will be referred to as $OH\cdots O$ from now on). Therefore, we calculated the radial distribution functions describing these pairs and examined the formation of the pertinent types of hydrogen bonds. The identification of a hydrogen bond was based on the hydrogen−acceptor distance as well as the angle formed by the donor−hydrogen−acceptor triplet. The distance corresponding to the first minimum of the respective hydrogen−acceptor pair distribution function was taken as the maximum separation between the hydrogen and the acceptor, whereas the minimum donor−hydrogen−acceptor angle was selected to be 120°.[46,64,65]

To examine the dynamics of hydrogen-bonding pairs at a wider temporal window, we also produced trajectories and collected data every 2 fs at the subpicosecond range. We investigated hydrogen-bonded pair dynamics by evaluating a survival probability function defined as[66,67]

$$P(t) = \frac{\sum_{(i,j)} p_{ij}(t)}{\sum_{(i,j)} p_{ij}(t=0)} \qquad (4)$$

where $p_{ij}(t)$ takes the value of 1 if the hydrogen bond that exists between the ith and the jth atoms at $t = 0$ exists also at time $t > 0$ and 0 otherwise. The summation runs over all atomic pairs found to form a hydrogen bond at $t = 0$ (all different time origins have been taken into account). According to this definition (usually referred to as "intermittent"[66]), all hydrogen formation/breaking events in a hydrogen−acceptor pair that existed at time $t = 0$ are not counted if they take place at times shorter than t; therefore, this definition reflects the long-time behavior of the hydrogen-bond-formation probability function.

3.2.1. Intramolecular Hydrogen Bonding. Figure 8 depicts the pair distribution functions utilized for the detection of $OH\cdots OH$ hydrogen bonds together with the corresponding survival correlation functions (eq 3) as a function of temperature. Following the criteria mentioned earlier, an intense hydrogen-bond peak can be readily identified in both systems at a separation of ~2 Å.

The amplitude of the hydrogen-bond peak (indicating the relative frequency of appearance of the examined pair) decreases upon an increase in temperature. It must be noted that even at the highest examined temperature, the hydrogen bond peak remains present. Actually, as shown by the survival correlations functions (Figure 8 insets), the long-time probability of hydrogen bonding between $OH\cdots OH$ pairs is not vanished at high temperatures, even on the longest time scales examined (i.e., they last longer than the nanosecond scale). Comparison of the survival correlation functions describing the two systems shows that the H20 polyester exhibits a lower degree of decorrelation than that observed in the H30 systems at similar temperatures.

The analogous picture for the $OH\cdots O$ intramolecular pairs is presented in Figure 9.

Apart from the hydrogen-bond peak that can be identified close to a separation of 2 Å, as in the case of $OH\cdots OH$, a distinct feature is the appearance of a second sharp maximum close to a distance of $r \cong 4.2$ Å between the carbonyl oxygen and the hydroxyl hydrogen in both systems studied. This feature appears to be consistent with the presence of a different kind of hydrogen bond, namely, of the $C{=}O\cdots OH\cdots HO$ type, where the distance between the hydrogen of the second hydroxyl group and the carbonyl oxygen gives rise to the second peak in the $g(r)$ spectra of Figure 9. (A peak at a separation of $r \cong 4.4$ Å was also noted in the corresponding carbonyl oxygen−hydroxyl oxygen pair correlation functions, not shown here.) The existence of such a "double" hydrogen bond has been hypothesized on account of some strong indications from infrared spectroscopic experiments in hyperbranched polyesters similar to the ones studied here.[56] Our findings corroborate this hypothesis. Another distinct feature in the behavior of the two systems is that the amplitude (i.e., the area under the maximum) of the peak assigned to the $OH\cdots OH$ hydrogen bond appears to decrease upon the decrease in temperature in the H30 model, whereas that of the second peak follows an

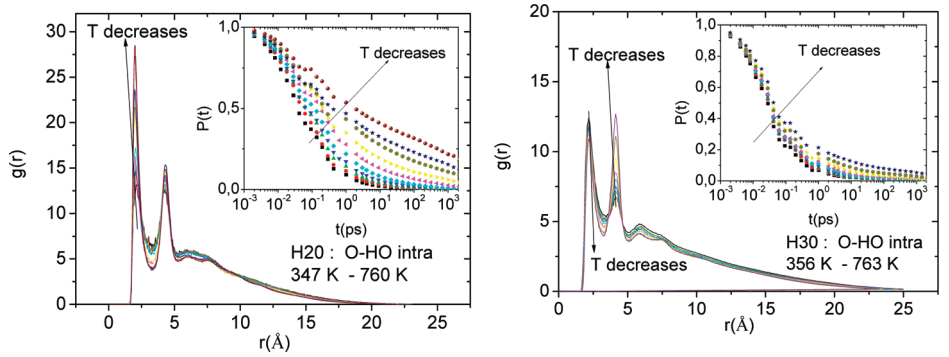

Figure 9. Intramolecular pair distribution functions between hydroxyl hydrogens and carbonyl oxygens for H20 (left, 347−760 K) and the H30 (right, 356−763 K) models as a function of temperature. Insets denote the corresponding survival correlations functions (eq 4). Arrows show the direction of the decrease in temperature.

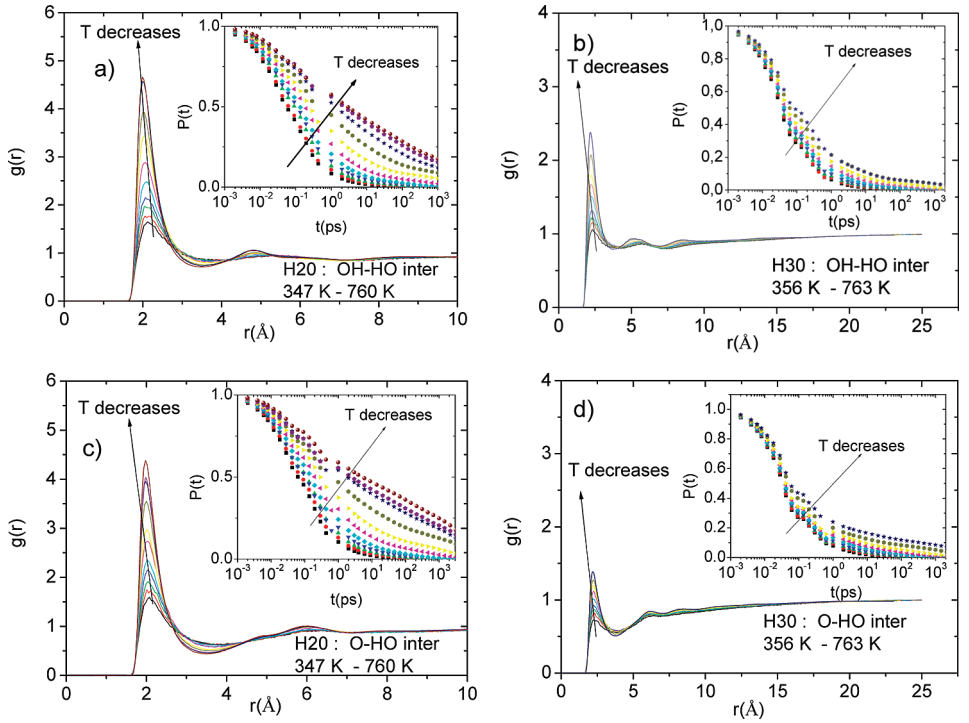

Figure 10. Intermolecular radial distribution functions for (a,b) the $OH\cdots OH$ and the $OH\cdots O$ pairs in (a,c) the H20 and (b,d) the H30 models. Insets display the corresponding hydrogen-bond survival correlation functions. Arrows denote the directions of the decrease in temperature.

inversely proportional relation. In the H20 model, although the primary maximum assumes higher values as the temperature drops, it also becomes narrower so that its amplitude does not change appreciably with temperature. The amplitude of the peak at $r \cong 4.2$ Å does not vary systematically with temperature as well. This observation implies that at the H30 polyester, the relative frequency of appearance of the assumed $C{=}O\cdots OH\cdots HO$ hydrogen bond increases as the temperatures lowers at the expense of the $OH\cdots OH$ pairs. Such a distinct behavior noted between the two pseudogenerations emphasizes the role that the topology might play in the hydrogen-bonding properties of a hyperbranched polymer.

Comparing the survival probability functions describing the two systems, we observe that they appear to decay slower in the H20 polyester at comparable temperatures, as was the case in the comparison of the $OH\cdots OH$ intramolecular bond. Actually, the survival correlation functions of the H30 model appear to decay in a particularly short time. (Compare the relative behavior in the insets of Figures 8 and 9.) The latter appear to have relaxed within the examined window, even at the lower temperature shown (i.e., its time scale is in the nanosecond range).

3.2.2. Intermolecular Hydrogen Bonding. For each of the H20 and H30 systems, the intermolecular hydrogen-bonding behaviors between the two examined pairs bear strong similarities, as can be inferred from Figure 10 (compare Figure 10a with Figure 10c and Figure 10b with Figure 10d). It is noteworthy that the additional peak observed in the intramolecular behavior of the $OH\cdots O$ pairs (Figure 9) is absent from the respective intermolecular pairs. In other words, the hydrogen bond of the $C{=}O\cdots OH\cdots HO$ type appears to be an exclusively intramolecular feature. The faster decorrelation of the hydrogen bond survival function previously observed in the corresponding intramolecular pairs of the larger generation model (Figures 8 and 9) characterizes the intermolecular behavior as well (compare inset of Figure 10a with that of Figure 10b and the inset of Figure 10c with that of Figure 10d).

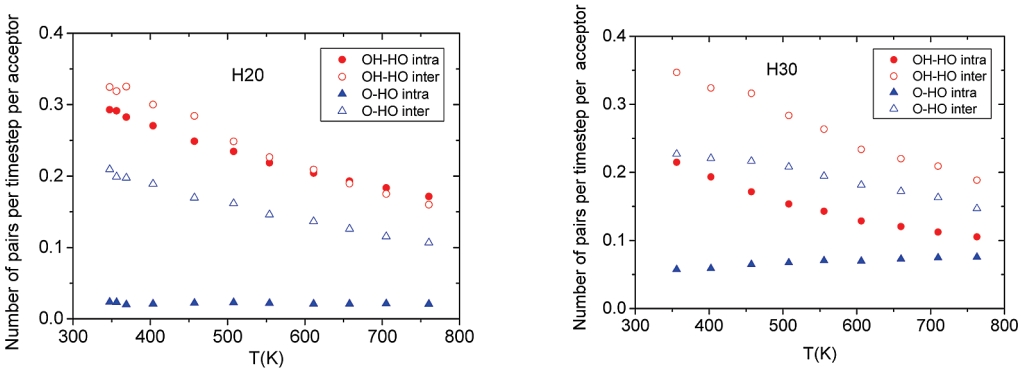

Figure 11. Average number of the examined hydrogen-bonded pairs per frame per acceptor atom for the H20 (left) and the H30 (right) models.

3.2.3. Numbers and Time Scales of the Examined Hydrogen Bonds. To better assess the relative significance of each kind of hydrogen bond in the two systems, we have estimated the average number of each kind per simulation frame (the frames considered are 1000 simulation steps apart) per donor atom, as shown in Figure 11.

A general remark is that the $OH\cdots OH$ pair is the dominant (taking into account both the intra- and the intermolecular contributions) kind of hydrogen bond formed in the examined systems. Between the hydrogen bonding behavior of the two pseudogenerations, several differences can be noted. The most striking feature is that the H20 polyester forms about 40 to 70% (depending on the temperature) more intramolecular $OH\cdots OH$ bonds than the H30 system. The levels of intermolecular bonds of the latter type are quite comparable. On the contrary, it appears that a higher number of $OH\cdots O$ hydrogen bonds, either of intra- or of intermolecular nature, are formed in the H30 polyester, particularly at higher temperatures.

Both of the above notions are consistent with experimental observations, where it was noted that formation of $OH\cdots OH$ hydrogen bonds is favored at short annealing times and low pseudogenerations of such polyesters,[18] whereas $OH\cdots O$ hydrogen bonds appeared to increase in higher generation analogues and at higher temperatures.[39] Specifically for the $OH\cdots O$ type of hydrogen bond, our results indicate a moderate increase in the intramolecular hydrogen bonds upon elevation of temperature. Although the degree of this augmentation does not exceed a percentage of 25% within a 400 K temperature interval, such a behavior indicates that certain intramolecular rearrangements within the polymer (such motions can be facilitated at higher mobility states, i.e., at higher temperatures) allow the realization of conformations that promote the formation of this type of intramolecular hydrogen bonds. The absence of such a behavior in the lower pseudogeneration polyester is likely to be the result of both the topological differences between the two polymers and the fact that the majority of the hydrogens belonging to hydroxyl groups prefer to form intramolecular hydrogen bonds with other hydroxyl oxygens of the $OH\cdots OH$ or of the $C{=}O\cdots OH\cdots HO$ type, as discussed above.

Figure 12 portrays the temperature dependence of the reciprocal relaxation times (see below) extracted from the corresponding survival correlation functions. To perform a fair comparison between the distinct kinds of bonds and for the different molecular weight systems (because in several cases, $P(t)$ functions do not reach full decorrelation within the simulation window), we chose to calculate the times at which the $P(t)$ spectra attain the same degree of decorrelation, here $1/e$. By making this selection, in the

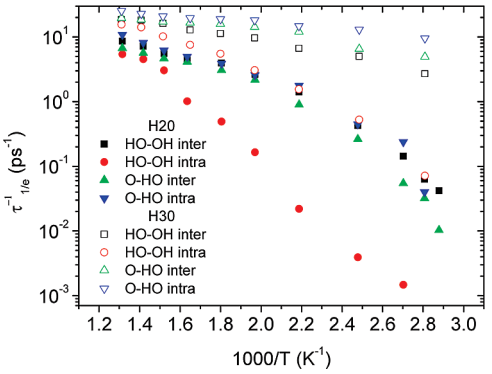

Figure 12. Relaxation rates calculated from the pertinent hydrogen-bonding survival correlations functions as discussed in the text.

examined cases, we essentially probe the initial relaxation rate rather than the longer time behavior of the survival function. Although this procedure will not map the actual survival times, which should also include the long-time behavior, it may well capture the relevant trends at least as far as it concerns time scales close to the nanosecond range.

As expected from the preceding discussion in Sections 3.2.1 and 3.2.2, for all types of hydrogen bonds, H20 exhibits lower relaxation rates compared with those observed in the H30 polyester. This difference in relaxation rates reaches almost two decades at lower temperatures. An additional feature shared by the two systems, is that the lowest rate corresponds to the intramolecular $OH\cdots OH$ hydrogen bond. For the higher generation molecule, apart from the intramolecular $OH\cdots OH$ bond, all hydrogen-bonded pairs exhibit a weak temperature variation of their relaxation rates, which correspond to characteristic times on the subpicosecond scale. The $OH\cdots OH$ intramolecular pair for the H20 model attains the picosecond or the 10 ps time scale depending on the temperature. For the lower generation model, the relaxation time of the intramolecular $OH\cdots OH$ pair reaches the nanosecond scale at the lowest examined temperature. The fact that the majority of the intramolecular hydrogen bonds are of the $OH\cdots OH$ type in the H20 model combined with its markedly low relaxation rate (compared with the other types of hydrogen bonds as well as with its H30 counterpart) implies a much slower rearrangement of the intramolecular hydrogen-bond network in this polyester.

This conclusion offers a strong basis for the interpretation of the picture described by dielectric relaxation experiments[41,42] performed in different pseudogenerations of hyperbranched polyesters similar to the ones examined in

this work. In one of these studies,[41] it was suggested that the motion of the hydroxyl groups, specifically in the H20 sample (as this was compared with the behavior of higher pseudogeneration molecules), is significantly hindered because of the formation of additional hydrogen bonding. In more recent dielectric measurements performed in a series of hyperbranched polyesters (second to fifth pseudogeneration) analogous to those studied here,[42] it was noted that the γ-relaxation, which was assigned to hydroxyl-group motion, exhibited considerably slower dynamics in the H20 sample compared with the same type of motion in higher generation systems. The authors conjectured that this effect was related to stronger intramolecular rather than intermolecular interactions involving the hydroxyl groups in the lower generation polyester.

In view of the above findings, that is, the higher degree of intramolecular $OH\cdots OH$ hydrogen bonding observed in the H20 model combined with the slower dynamics of the resulted hydrogen-bond network, one can rationalize the slower relaxation of bonds involving the hydroxyl oxygens, as discussed in Sections 3.1.2 and 3.1.3, by considering a coupling mechanism between the bond reorientational motion and the dynamics related to the survival of the formed hydrogen bonds. This scenario appears to be consistent with the aforementioned experimental results.

3.3. Overview of Local Dynamics. Figure 13 compares the relaxation rates of the bond reorientational dynamics discussed in Section 3.1. For a better assessment of the relative time scales characterizing the examined molecules, we have also included average reciprocal times from the overall rotational motion of the polymers. (See the Appendix.) The inset presents the inverse times corresponding to the slow process of the C−O bond reorientation (Figure 6) at temperatures at which this could be clearly resolved. Together, the average reciprocal times of the same motion as well as the relaxation rates describing overall molecular rotation for the two models are repeated from the main panel of the Figure to facilitate visual comparison.

Comparing the general behavior of the H20 and H30 molecules, it can be noticed that in the larger size systems the average relaxation rates are ordered in a hierarchical manner, in the sense that the backbone bond (C−C) clearly assumes the lower rate; then, the bond belonging to the side group (C−OH) is the next fastest, whereas the fastest motion corresponds to the bond possessing the larger orientational freedom, that is, the HO−OH bond. In the H20 system, a similar clear distinction between the C−C and the C−O bonds is not observed. Instead, these two bonds assume very similar rates. Another feature characterizing the general comparison of the dynamic behavior between the two systems is that they exhibit very close time scales for the overall rotational motion (i.e., the G_V rates) despite the fact that the average size of the molecules is different. (See Figure 2.) This proximity in the molecular rotation rates could actually rationalize the similarity of the C−C bond dynamics in the two systems. This type of bond is expected to be coupled to a larger extent to the reorientation of the "arm" it belongs in (Figure 1) and therefore to the overall molecular reorientation.

For the rest of the bonds examined, dynamics in the H20 system appear to be distinctly slower (on the order of one decade) compared with their H30 analogues. This can be understood in terms of a coupling to the slower hydrogen-bond dynamics of intramolecular origin, as was previously suggested. Coupling of the C−OH bond motion to the overall rotation appears to be stronger in the H20 model, as can be inferred by the close proximity of the relaxation rates corresponding to the slow dynamic process (Figure 13 inset) resolved in the lower temperatures (Figure 6) with those of the global rotational motion. Note that an analogous comparison cannot be made for the C−C bond because the three peaks are not clearly resolved in the corresponding DRTs. (See Figure 5.)

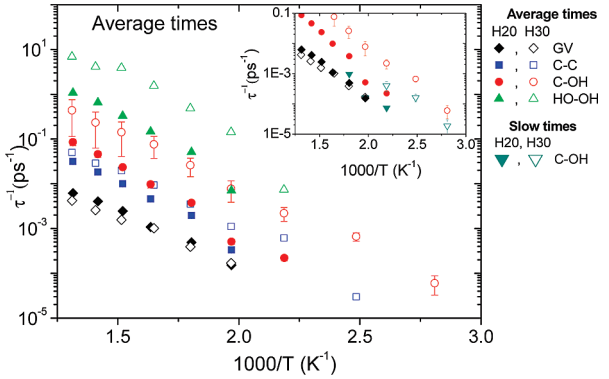

Figure 13. Relaxation map of the examined bond reorientational dynamics. GV stands for the $G_V(t)$ average reciprocal time scales. (See the Appendix.) The rates describing the HO−OH bond were calculated by integration of the respective correlation functions (Figure 7). The inset includes the reciprocal relaxation times of the slow process resolved in the C−OH bond dynamics (Figure 6).

4. Summary/Conclusions

In this work, we have examined local dynamics and hydrogen-bonding characteristics of hyperbranched hydroxyl-terminated polyesters in the molten state, bearing structures corresponding to the topologies of the commercially available H20 and H30 (Boltorn) systems. Our aim was to offer new insight into the mechanisms that govern local dynamic behavior of these systems and particularly on their relation to the hydrogen-bonding properties, thus facilitating the interpretation of relevant experimental findings. To the authors' knowledge, this is the first fully atomistic simulational approach of these scientifically interesting and commercially important systems, which attempts a description of their local dynamic properties at this level of detail. On the basis of this approach, we have been able to provide a qualitative and a partially quantitative account of the characteristics of the formed hydrogen-bonding network as well as of the degree that these hydrogen-bonding properties affect the local dynamic response.

From our results, it became apparent that the topology of the hyperbranched polymer plays a significant role in its physical behavior down to the atomic level. More specifically, it was found that the lower pseudogeneration polyester H20 assumed significantly slower dynamics of bonds that constituted by atoms involved in hydrogen bonds. The main feature that differentiated its behavior from the higher generation polyester appeared to be the considerably higher degree of intramolecular hydrogen bonding between hydroxyl hydrogens and hydroxyl oxygens. Although this type of hydrogen bond was found to be the most abundant in both size systems, the average number of intramolecular $OH\cdots OH$ pairs in H20 polyester was found to be 40−70% (depending on temperature) higher compared with that observed in the H30 system. This incidence should apparently be related to the differences in the structural details of the two systems. (See Figure 1.) The higher abundance of $OH\cdots OH$ bonds in the smaller size model combined with the longer survival time of this kind of hydrogen bond appeared to slow-down local reorientation

of bonds formed by hydroxyl hydrogens and hydroxyl oxygens significantly. This finding offers a new basis for the interpretation of relevant experimental observations, where it was noted that the dynamics of the hydroxyl groups, which was associated with the γ-relaxation process, exhibited the characteristics of a more constricted or more cooperative motion in the H20 polyester compared with that detected in the H30 or higher generation polyesters of the same family, which was not expected on the basis of the local nature of the motion and on the behavior of the dynamics of the −OH group in other polymers.

In addition, findings from our simulations corroborate the existence of the $C{=}O\cdots OH\cdots HO$ type of intramolecular hydrogen bonds in these systems, which was recently proposed on the basis of indications from infrared spectroscopy experiments. Actually, (on account of the relative amplitude of the pertinent peaks, see Figure 9) the formation of this kind of multiple hydrogen bonding was found to be favored in the larger size model and to depend sensitively on temperature changes, in contrast with the behavior observed in the lower generation system.

In conclusion, we believe that the detail afforded by this kind of simulations and analysis approach, is necessary for a more profound understanding of the mechanisms that operate at the atomic level and may significantly affect the physical properties of such systems.

Acknowledgment. This research project is cofinanced by E. U.-European Social Fund (75%) and the Greek Ministry of Development-GSRT (25%) under the EU/GSRT PENED 2003 grant no. 03EΔ716. The present work is also performed in the framework of the European Science Foundation COST TD0802 action.

Appendix

To examine dynamics associated with the overall rotational motion of the molecule, we have calculated the second-order Legendre polynomial

$$G_V(t) = \frac{1}{2}\langle 3[\hat{h}(t)\cdot\hat{h}(0)]^2 - 1\rangle \qquad \text{(A1)}$$

of unit vectors , which connect the center of mass of each molecule to the individual atoms. Such a correlation function essentially relaxes via the reorientational motion of the entire molecule.[47]

Figure A1 presents $G_V(t)$ for the two examined systems. Average relaxation times, as presented in Figure 13, were calculated by integrating the corresponding DRTs only for temperatures at which a substantial degree of decorrelation was reached within the examined temporal window.

Note Added after ASAP Publication. This article posted ASAP on November 2, 2009. Various text changes have been made throughout the paper. The correct version posted on November 5, 2009.

References and Notes

(1) Hult, A.; Johansson, M.; Malmstrom, E. *Adv. Polym. Sci.* **1999**, *143*, 1.
(2) Voit, B. I. *C. R. Chim.* **2003**, *6*, 821–832.
(3) Gong, W.; Mai, Y. Y.; Zhou, Y. F.; Qi, N.; Wang, B.; Yan, D. Y. *Macromolecules* **2005**, *38*, 9644–9649.
(4) Koslowski, T.; Jurjiu, A.; Blumen, A. *Macromol. Theory Simul.* **2006**, *15*, 538–545.
(5) Dalakoglou, G. K.; Karatasos, K.; Lyulin, S. V.; Lyulin, A. V. *J. Chem. Phys.* **2007**, *127*, 214903.
(6) Kharchenko, S. B.; Kannan, R. M.; Cernohous, J. J.; Venkataramani, S. *Macromolecules* **2003**, *36*, 399–406.
(7) Kharchenko, S. B.; Kannan, R. M.; Cernohous, J. J.; Venkataramani, S.; Babu, G. N. *J. Polym. Sci., Part B: Polym. Phys.* **2001**, *39*, 2562–2571.
(8) Luciani, A.; Plummer, C. J. G.; Nguyen, T.; Garamszegi, L.; Manson, J. A. E. *J. Polym. Sci., Part B: Polym. Phys.* **2004**, *42*, 1218–1225.
(9) Klajnert, B.; Bryszewska, M. *Dendrimers in Medicine*; Nova Science Publishers: New York, 2007.
(10) Saville, P. M.; Reynolds, P. A.; White, J. W.; Hawker, C. J.; Frechet, J. M. J.; Wooley, K. L.; Penfold, J.; Webster, J. R. P. *J. Phys. Chem.* **1995**, *99*, 8283–8289.
(11) Plummer, C. J. G.; Luciani, A.; Nguyen, T.-Q.; Garamszegi, L.; Rodlert, M.; Manson, J.-A. E. *Polym. Bull.* **2002**, *49*, 77–84.
(12) Mackay, M. E.; Carmezini, G. *Chem. Mater.* **2002**, *14*, 819–825.
(13) Peleshanko, S.; Tsukruk, V. V. *Prog. Polym. Sci.* **2008**, *33*, 523–580.
(14) Freire, J. J. *Soft Matter* **2008**, *4*, 2139–2143.
(15) Connolly, R.; Timoshenko, E. G.; Kuznetsov, Y. A. *Macromolecules* **2004**, *37*, 7381.
(16) Lee, H.; Baker, J. R.; Larson, R. G. *J. Phys. Chem. B* **2006**, *110*, 4014–4019.
(17) Suek, N. W.; Lamm, M. H. *Macromolecules* **2006**, *39*, 4247–4255.
(18) Zagar, E.; Huskic, M.; Zigon, M. *Macromol. Chem. Phys.* **2007**, *208*, 1379–1387.
(19) Tande, B. M.; Wagner, N. J.; Kim, Y. H. *Macromolecules* **2003**, *36*, 4619–4623.
(20) Malmström, E.; Hult, A.; Gedde, U. W.; Liu, F.; Boyd, R. H. *Polymer* **1997**, *38*, 4873–4879.
(21) Gao, F.; Schricker, S. R.; Tong, Y.; Culbertson, B. M. *J. Macromol. Sci., Pure Appl. Chem.* **2002**, *39*, 267.
(22) Borah, J.; Mahapatra, S. S.; Saikia, D.; Karak, N. *Polym. Degrad. Stab.* **2006**, *91*, 2911–2916.
(23) Zimmerman, S.; Lawless, L. *Top. Curr. Chem.* **2001**, *217*, 95–120.
(24) Giupponi, G.; Buzza, D. M. A. *J. Chem. Phys.* **2005**, *122*, 194903.
(25) Jiang, G. H.; Wang, L.; Yu, H. J.; Chen, C.; Dong, X. C.; Chen, T.; Yang, Q. *Polymer* **2006**, *47*, 12–17.
(26) Ornatska, M.; Bergman, K. N.; Goodman, M.; Peleshanko, S.; Shevchenko, V. V.; Tsukruk, V. V. *Polymer* **2006**, *47*, 8137–8146.
(27) Smirnova, N. N.; Stepanova, O. V.; Bykova, T. A.; Markin, A. V.; Muzafarov, A. M.; Tatarinova, E. A.; Myakushev, V. D. *Thermochim. Acta* **2006**, *440*, 188.
(28) Perstorp. http://www.perstorp.com/.

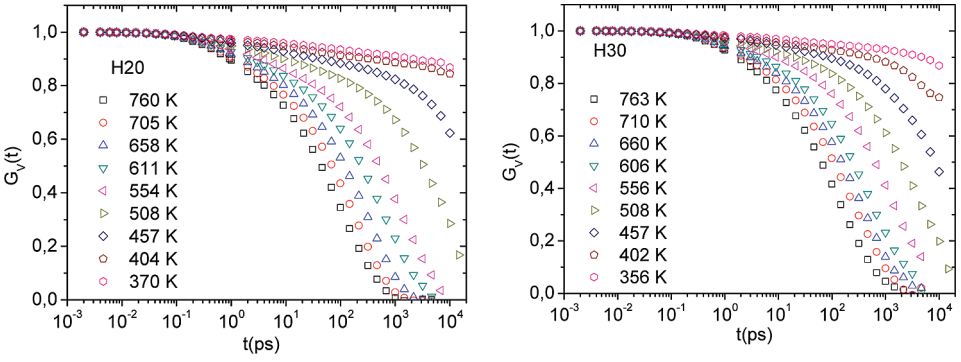

Figure A1. Correlation functions describing the global rotational motion of the polyester molecules (eq 5) for the H20 (left) and the H30 (right) models.

(29) Malmström, E.; Johansson, M.; Hult, A. *Macromolecules* **1995**, *28*, 1698–1703.
(30) Jena, K. K.; Raju, K. V. S. N.; Prathab, B.; Aminabhavi, T. M. *J. Phys. Chem. B* **2007**, *111*, 8801–8811.
(31) Sterescu, D. M.; Stamatialis, D. F.; Mendes, E.; Kruse, J.; Ratzke, K.; Faupel, F.; Wessling, M. *Macromolecules* **2007**, *40*, 5400–5410.
(32) Arce, E.; Nieto, P. M.; Diaz, V.; Castro, R. G.; Bernad, A.; Rojo, J. *Bioconjugate Chem.* **2003**, *14*, 817–823.
(33) Zou, J. H.; Shi, W. F.; Wang, J.; Jun, B. *Macromol. Biosci.* **2005**, *5*, 662–668.
(34) Leinweber, D.; Feustel, M.; Wasmund, E.; Rausch, H. Alkoxylated Dendrimers and Use Thereof As Biodegradable Demulsifiers. U.S. Patent 7,569,615, Aug 4, **2009**.
(35) Czech, P.; Okrasa, L.; Ulanski, J.; Boiteux, G.; Mechin, F.; Cassagnau, P. *J. Appl. Polym. Sci.* **2007**, *105*, 89–98.
(36) Malmström, E.; Liu, F.; Boyd, R. H.; Hult, A.; Gedde, U. W. *Polym. Bull.* **1994**, *32*, 679–685.
(37) Hsieh, T. T.; Tiu, C.; Simon, G. P. *Polymer* **2001**, *42*, 1931–1939.
(38) Zagar, E.; Zigon, M. *Macromolecules* **2002**, *35*, 9913–9925.
(39) Zagar, E.; Huskic, M.; Grdadolnik, J.; Zigon, M.; Zupančič-Valant, A. *Macromolecules* **2005**, *38*, 3933–3942.
(40) Zagar, E.; Zigon, M.; Podzimek, S. *Polymer* **2006**, *47*, 166–175.
(41) Zhu, P. W.; Zheng, S.; Simon, G. *Macromol. Chem. Phys.* **2001**, *202*, 3008–3017.
(42) Turky, G.; Shaaban, S. S.; Schöenhals, A. *J. Appl. Polym. Sci.* **2009**, *113*, 2477–2484.
(43) *Cerius 2 Package*; Accelrys, http://www.accelrys.com.
(44) Weiner, S. J.; Kollman, P. A.; Nguyen, D. T.; Case, D. A. *J. Comput. Chem.* **1986**, *7*, 230–252.
(45) Posocco, P.; Ferrone, M.; Fermeglia, M.; Pricl, S. *Macromolecules* **2007**, *40*, 2257–2266.
(46) Lee, H.; Baker, J. R.; Larson, R. G. *J. Phys. Chem. B* **2006**, *110*, 4014–4019.
(47) Tanis, I.; Tragoudaras, D.; Karatasos, K.; Anastasiadis, S. H. *J. Chem. Phys. B* **2009**, *113*, 5356–5368.
(48) Mager, P. *Mol. Simul.* **1998**, *20*, 201.
(49) Nimmanpipug, P.; Lee, V.; Chaijaruwanich, J.; Prasitwattanaseree, S.; Traisathit, P. Structural Screening of HIV-1 Protease/Inhibitor Docking by Non-Parametric Binomial Distribution Test. In *Bioinformatics Research and Development*, Proceedings of the First International Conference, BIRD 2007, Berlin, Germany, March 2007; Hochreiter, S., Wagner, R., Eds.; Springer: New York, 2007; pp 119−130.
(50) Shimamoto, S.; Yoshida, T.; Inui, T.; Gohda, K.; Kobayashi, Y.; Fujimori, K.; Tsurumura, T.; Aritake, K.; Urade, Y.; Ohkubo, T. *J. Biol. Chem.* **2007**, *282*, 31373–31379.
(51) Gasteiger, J.; Marsili, M. *Tetrahedron* **1980**, *36*, 3219–3228.
(52) Gelin, B. R.; Karplus, M. *Biochemistry* (*Moscow, Russ. Fed.*) **1979**, *18*, 1256–1268.
(53) Weiner, S. J.; Kollman, P. A.; Case, D. A.; Singh, U. C.; Ghio, C.; Alagona, G.; Profeta, S.; Weiner, P. *J. Am. Chem. Soc.* **1984**, *106*, 765–784.
(54) CCLRC, Daresbury Laboratory, Daresbury, Warrington Wa4 4AD, England. The simulations were performed by utilization of an appropriately modified version of the DL_POLY package. DL_POLY is a parallel molecular dynamics package developed at Daresbury laboratory and is property of the Council for the Central Laboratory of the Research Councils (CCLRC) (T. Forester and W. Smith).
(55) Seiler, M.; Rolker, J.; Mokrushina, L.; Kautz, H.; Frey, H.; Arlt, W. *Fluid Phase Equilib.* **2004**, *221*, 83.
(56) Zagar, E.; Grdadolnik, J. *J. Mol. Struct.* **2003**, *658*, 143–152.
(57) Provencher, S. *Comput. Phys. Commun.* **1982**, *27*, 229.
(58) Provencher, S. A General-Purpose Constrained Regularization Method for Inverting Photon Correlation Data. In *Photon Correlation Techniques in Fluid Mechanics*, Proceedings of the 5th International Conference at Kiel-Dampl, Fed. Rep. Germany, May 23−26, 1982; Schulz-DuBois, E. O., Ed.; Springer-Verlag: Berlin, 1983.
(59) Emran, S. K.; Newkome, G. R.; Weis, C. D.; Harmon, J. P. *J. Polym. Sci., Part B: Polym. Phys.* **1999**, *37*, 2025–2038.
(60) Karatasos, K. *Macromolecules* **2006**, *39*, 4619.
(61) Karatasos, K. *Macromolecules* **2005**, *38*, 4472.
(62) Karatasos, K.; Anastasiadis, S. H.; Fytas, G.; Semenov, A. N.; Pitsikalis, M.; Hadjichristidis, N. *Macromolecules* **1994**, *27*, 3543.
(63) Karatasos, K.; Ryckaert, J. P. *Macromolecules* **2001**, *34*, 7232–7235.
(64) Chiessi, E.; Cavalieri, F.; Paradossi, G. *J. Phys. Chem. B* **2007**, *111*, 2820–2827.
(65) Jeffrey, G. A.; Saenger, W. *Hydrogen Bonding in Biological Structures*; Springer-Verlag: Berlin, 1991.
(66) Rapaport, D. C. *Mol. Phys.* **1983**, *50*, 1151–1162.
(67) Swiatla-Wojcik, D. *Chem. Phys.* **2007**, *342*, 260–266.